Kinetics and Catalysis, Vol. 43, No. 3, 2002, pp. 384–390. Translated from Kinetika i Kataliz, Vol. 43, No. 3, 2002, pp. 415–421.

The Structure of Oxide Ga–Sb–Ni–P–W–O/SiO_2 Catalyst and Its Catalytic Properties in Propane Ammoxidation

G. A. Zenkovets, G. N. Kryukova, S. V. Tsybulya, V. F. Anufrienko, T. V. Larina, and E. B. Burgina

Boreskov Institute of Catalysis, Siberian Division, Russian Academy of Sciences, Novosibirsk, 630090 Russia

Received June 19, 2001

Abstract—The structure of the multicomponent catalyst $Ga_1Ni_1P_2W_{0.5}Sb_6O_x/SiO_2$ and its catalytic properties in propane ammoxidation are studied. The catalyst is nanostructured and consists of noncoherently spliced blocks of a multiply promoted phase with a structure of gallium antimonate, which covers SiO_2 particles with a thin layer. In the multiply promoted compound with a structure of gallium antimonate, Ni^{2+} ions partially substitute for Ga^{3+} and W^{6+} ions partially substitute for Sb^{5+}. This leads to an increase in the crystalline lattice parameters *a* and *c*. Phosphate ions are stabilized in the region of block interfaces. The catalyst is characterized by high efficiency in propane ammoxidation.

INTRODUCTION

Propane ammoxidation to acrylonitrile is one of the promising processes of organic synthesis due to its low cost, the accessibility of the starting materials, and the broad commercial use of acrylonitrile [1]. Therefore, for the last 30 years, a search for a highly efficient catalyst for this process has been underway. From 1970, many patents and research publications have been devoted to the development and study of new catalysts. It has been shown that antimony-containing catalysts show high activities and selectivities in propane ammoxidation [1–13].

Vanadium–antimony catalysts, binary or alumina-supported, are the most studied. These are mixtures of vanadium antimonate rutile phases and antimony oxide α-Sb_2O_4 [1, 3–13]. Structural studies of these catalysts by high-resolution electron microscopy [13] showed that antimony oxide, which is a component of vanadium–antimony catalysts, is a nanostructured material, because a single particle of this oxide consists of alternating regions of different modifications: α-Sb_2O_4 and β-SbO_4. The yield of acrylonitrile on these catalyst is ~20% (single pass) or ~35–39% (recycle).

It is known that Sn–Sb–O [14], Sn–V–Sb–O [15–17], Ni–V–Sb–O [2], and Ga–Sb–O [18–22] catalysts are also active in propane ammoxidation. The properties of multiply promoted Ga–Sb–Ni–P–*M* (*M* = La, Mo, and W) catalysts were described in [23–25]. These are active and selective in the ammoxidation of the propane–propylene mixtures containing 4.5% propane and 0.5% propylene. The highest acrylonitrile yield (~50%) is achieved when the catalyst contains tungsten. According to Burylin *et al.* [24], these catalysts are prepared by coprecipitation with ammonia from the salts of initial components and contain three phases: gallium antimonate, nickel antimonate, and X-ray amorphous P–Sb compound.

It is known that the preparation procedure substantially affects the extent of interaction between the components and the phase composition, especially in the case of multicomponent systems. In connection with this, it is interesting to study the phase composition and structure of multicomponent Ga–Sb–Ni–P–W–O/SiO_2 catalyst prepared by the mixing method. This method is promising for environmental reasons because it eliminates sewage containing antimony and other heavy metals involved in the catalyst composition.

This paper deals with the structure of the multicomponent oxide Ga–Sb–Ni–P–W–O/SiO_2 catalyst obtained by the mixing method and its catalytic properties in propane ammoxidation.

EXPERIMENTAL

A $Ga_1Ni_1P_2W_{0.5}Sb_6O_x/SiO_2$ catalyst containing 30 wt % SiO_2 was prepared by mixing an X-ray amorphous P–Sb compound with a Sb : P ratio of 3 : 1 with aerosil SiO_2 and solutions of the following salts: gallium nitrate, nickel nitrate, and ammonium tungstate. The resulting suspension was dried in an Anhydro-type spray drier to obtain powder, which was then pelletized and ground to obtain a 1.0–0.5 mm fraction. The latter was dried in air at 110°C for 12 h and calcined in a muffle furnace at 750°C for 4 h.

A sample of pure gallium antimonate $GaSbO_4$ was prepared by coprecipitation from a solution of gallium nitrate and antimony pentachloride with an ammonia solution at constant pH 7 and 70°C. The precipitate was washed with distilled water, dried in air to the air-dry state and then in a desiccator at 110°C, and calcined in air at 750°C for 4 h.

0023-1584/02/4303-0384$27.00

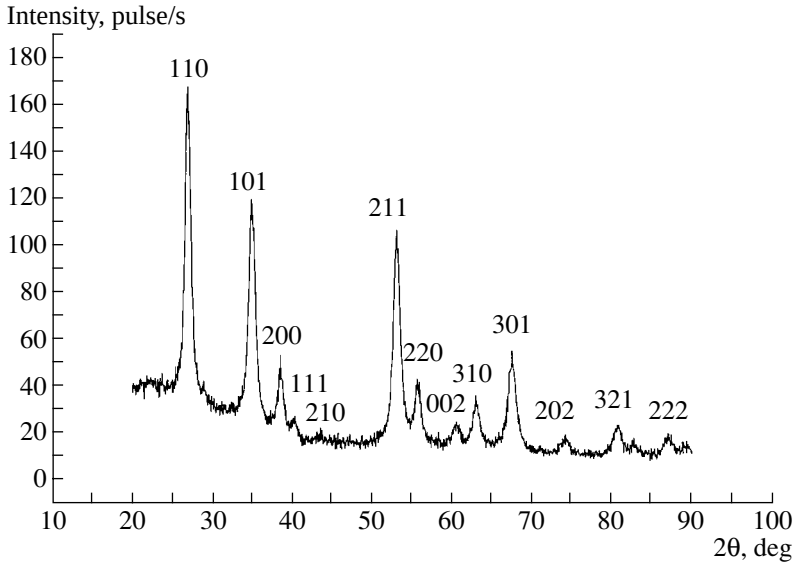

Fig. 1. XRD patterns of the $Ga_1Ni_1P_2W_{0.5}Sb_6O_x/SiO_2$ catalyst.

P–Sb samples with different P : Sb ratios were prepared according to the procedure described in [26].

X-ray analyses of the samples were carried out using a URD-63 diffractometer (CuK_α radiation) equipped with a graphite monochromator. XRD patterns were obtained by scanning with a step of 0.05° and a signal accumulation time of 20 s in the range of angles 20°–90°. Lattice parameters were refined by the least-squares method (10 signals) using a program [27]. The size of coherent scattering regions (CSR) was estimated according to the Selyakov–Shearer formula [28] using diffraction peak 1.1.0.

Electron microscopic studies were carried out using a JEM-2010 instrument with a resolution of 0.14 nm and an accelerating voltage of 200 kV.

IR spectra were recorded with a BOMEM MB-102 spectrometer. The sample for IR measurements were prepared according to the standard procedure: pellets were prepared that contained 2 mg of the catalyst and 500 mg KBr.

Diffuse-reflectance electron spectra were recorded using a two-beam UV-2501 PC spectrophotometer (Shimadzu) at wavelengths of 190–900 nm.

ESR spectra were recorded using a JES-3BX instrument at 77 and 300 K using DPPG as the standard.

The samples were tested in propane ammoxidation to acrylonitrile in a U-shaped Pyrex reactor with a height of 190 mm and a diameter of 5 mm. The catalyst sample (a 0.50–0.25 mm fraction) with a bed length-to-diameter ratio of 20–25 was heated in the flow of the reaction mixture to 550°C. The reaction mixture contained (vol %): 4.5 C_3H_8, 0.5 C_3H_6, 12 NH_3, 0.04 C_2H_5Br, 18.6 O_2, and 64.3 He. The components of the reaction mixture were analyzed by chromatography. Hydrocyanic acid was analyzed by titration with silver nitrate.

RESULTS AND DISCUSSION

According to XRD data, the $Ga_1Ni_1P_2W_{0.5}Sb_6O_x/SiO_2$ catalyst consists of one phase. This is a gallium antimonate compound with a rutile structure [29]. Figure 1 shows the XRD pattern of the catalyst, and it can be seen that there are no peaks corresponding to other phases.

Measurements of the lattice parameters of the studied catalyst showed that parameters *a* and *c* are higher than the corresponding parameters of gallium antimonate (Table 1). This can be due to the fact that Ga^{3+} or Sb^{5+} cations in the gallium antimonate are replaced by other cations with larger radii or to the formation of intercalation solid solution. The size of CSR of the multicomponent catalyst is 11 nm.

Figure 2 shows the diffuse-reflectance electron spectra of the studied catalyst and pure $GaSbO_4$. Two regions of absorption can be seen in the spectrum of the $Ga_1Ni_1P_2W_{0.5}Sb_6O_x/SiO_2$ catalyst: weak bands in the low-frequency region at 13000 and 15000 cm^{-1} (Fig. 2a) and a band in the margin of the UV region at 31000 cm^{-1}. The bands at 13000 and 15000 cm^{-1} are characteristic of *d–d* transitions of Ni^{2+} ions in the octahedral coordination [30]. According to [30], the ground state of the free Ni^{2+} ion (d^8) is the term ^3F, whereas in the crystalline field of the octahedral coordination, the main term is $^3A_{2g}$. Therefore, three spin-allowed transitions are observed: $^3A_{2g} \longrightarrow {}^3T_{2g}$, $A_{2g} \longrightarrow {}^3T_{1g}$, $^3A_{2g} \longrightarrow {}^3T_{1g}$ (P). These transitions are superimposed on spin-forbidden transitions $^3A_{2g} \longrightarrow {}^1E_g$ and

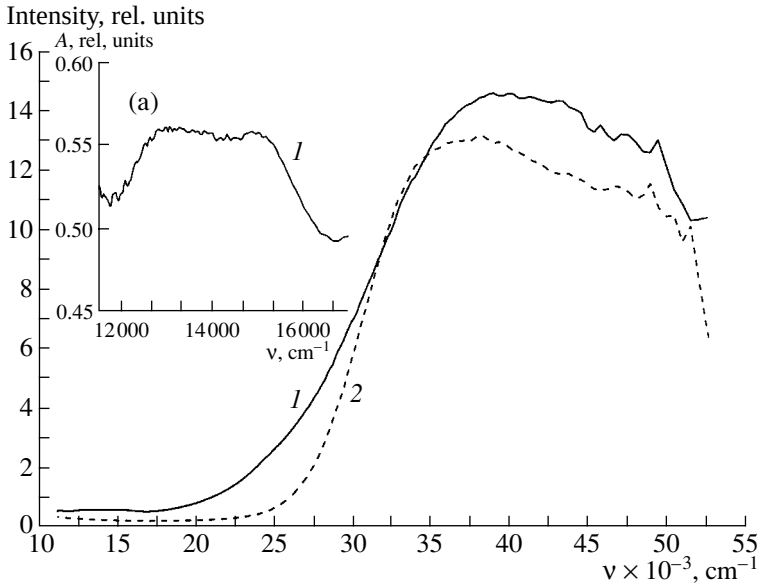

Fig. 2. Diffuse-reflectance electron spectra of (*1*) the $Ga_1Ni_1P_2W_{0.5}Sb_6O_x/SiO_2$ catalyst and (*2*) $GaSbO_4$. (a) The region of spectrum *1* at 12000–16000 cm^{-1}.

$^3A_{2g} \longrightarrow {}^1T_{2g}$. The valence transition $^3A_{2g} \longrightarrow {}^3T_{2g}$ is in the region of frequencies below 10000 cm^{-1} and cannot be observed in our experimental conditions, whereas the transition $^3A_{2g} \longrightarrow {}^1T_{2g}$ is weak and cannot be seen distinctly. Analysis of experimental data for the *d–d* transition for metal ions in an octahedral oxygen environment [31] shows that the apparent absorption bands of the Ni^{2+} ion are due to the transitions $^3A_{2g} \longrightarrow {}^1E_g$ (13000 cm^{-1}) and $^3A_{2g} \longrightarrow {}^3T_{1g}$ (15000 cm^{-1}). The transition $^3A_{2g} \longrightarrow {}^3T_{1g}$ (*P*) is in the UV range for this catalyst and is superimposed on the margin of rutile absorption range.

Analysis of the UV range of the spectrum of the $Ga_1Ni_1P_2W_{0.5}Sb_6O_x/SiO_2$ catalyst and pure $GaSbO_4$ (rutile) shows that the proper absorption edges practically coincide for these samples near 31000 cm^{-1}, which is typical of all rutile compounds [30]. These data confirm the results of XRD analysis suggesting that a rutile compound is formed in the multicomponent catalyst.

The ESR spectrum of tungsten ions did not contain signals from W^{5+} ions. Therefore, tungsten is in the state of W^{6+}.

Table 1. Crystalline lattice parameters of for $GaSbO_4$ and the $Ga_1Ni_1P_2W_{0.5}Sb_6O_x/SiO_2$ catalyst

Sample	*a*, Å	*c*, Å
$GaSbO_4$	4.600	3.034
$Ga_1Ni_1P_2W_{0.5}Sb_6O_x/SiO_2$	4.658	3.052

Based on diffuse-reflectance electron spectroscopic and ESR data, we assume that the Ni^{2+} ions are in octahedral coordination in the multicomponent catalyst and substitute for the Ga^{3+} ions, which also have an octahedral environment in the structure of gallium antimonate. Because the ionic radius of Ni^{2+} (0.69 Å) is larger than the radius Ga^{3+} (0.62 Å) [32], the substitution of 0.62 Å for gallium ions leads to an increase in the lattice parameters of gallium antimonate. This agrees with XRD data. Proceeding from the fact that Sb^{5+} and W^{6+} have similar octahedral oxygen environments and their radii are the same (0.62 Å) [32], we assume that the W^{6+} ions partially substitute for Sb^{5+} in the structure of gallium antimonate. Moreover, the above substitutions in the structure of a compound based on gallium antimonate preserve the overall electroneutrality of the system.

Figure 3 shows the IR spectra of the initial $Ga_1Ni_1P_2W_{0.5}Sb_6O_x/SiO_2$ catalyst (spectrum *2*), SiO_2 calcined at the same temperature as the catalyst (spectrum *1*), the difference spectrum of the catalyst and support (spectrum *3*), and the spectrum of $GaSbO_4$. In the difference spectrum (*3*), the absorption bands of SiO_2 at 1110, 807, and 474 cm^{-1} are nearly compensated, and we can reliably determine bands at 1006, 966, 883, 733, 700, 644, 562, and 331 cm^{-1}. Bands at 1162 and 480 cm^{-1} were determined less reliably, because an error in spectrum subtraction increases at the contours of intense bands. The difference spectrum (*3*) compared to the spectrum of pure gallium antimonate (*4*) shows that the main bands shift toward higher frequencies in the range of 500–780 cm^{-1}. This fact may point to a change in the *M*–O bond length in the multiply pro-

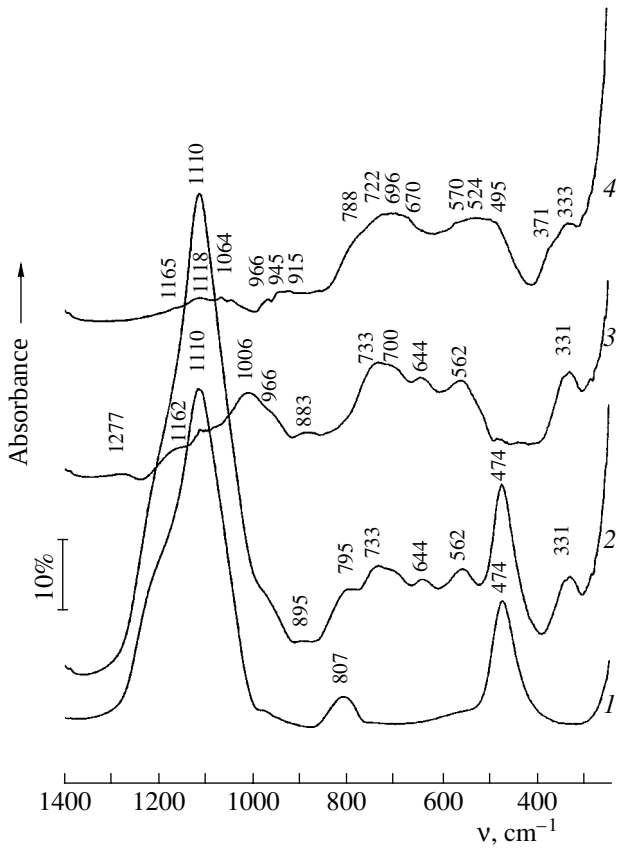

Fig. 3. IR spectra of (*1*) SiO_2 and (*2*) $Ga_1Ni_1P_2W_{0.5}Sb_6O_x/SiO_2$; (*3*) the difference spectrum of $Ga_1Ni_1P_2W_{0.5}Sb_6O_x/SiO_2$ and SiO_2; and (*4*) the spectrum of $GaSbO_4$.

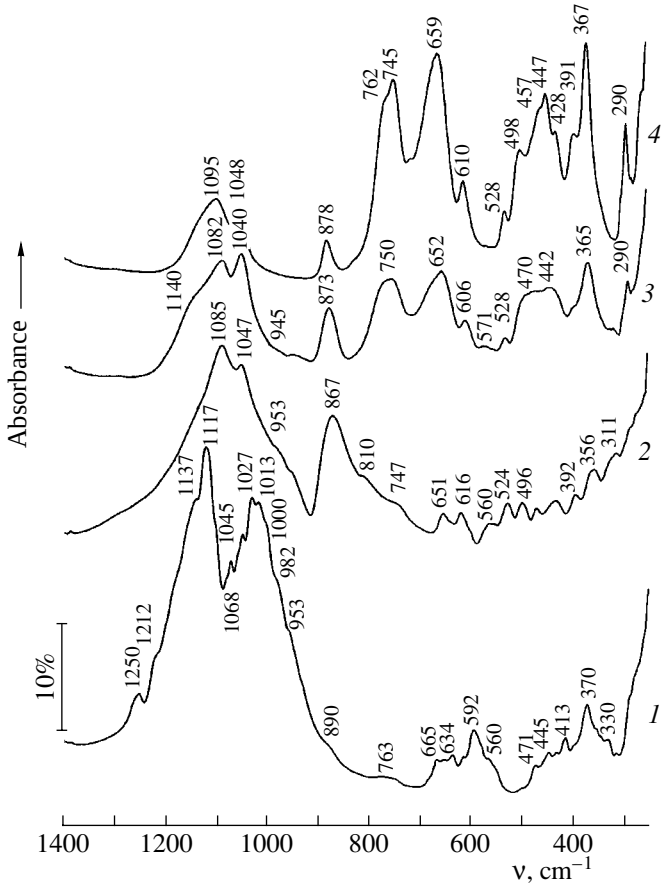

Fig. 4. IR spectra of P–Sb samples with the ratios: (*1*) Sb : P = 1 : 2, (*2*) 1 : 1, (*3*) 4 : 1, and (*4*) 15 : 1.

moted catalyst with a structure of gallium antimonate compared to pure gallium antimonate.

The difference spectrum also shows rather intense bands at 1162, 1006, 966, and 883 cm^{-1} in a range that is not typical of the structural type of gallium antimonate. Note that these bands do not coincide with those observed in the spectra of gallium and nickel phosphates [33]. To identify these bands, we recorded the spectra of model P–Sb–O samples with different Sb : P ratios. Figure 4 shows that a group of bands at 1250–890 cm^{-1} is certainly assignable to the stretching vibrations of the PO_4 tetrahedron. The band at 1250 cm^{-1} for the sample with substantial phosphorus excess (Sb : P = 1 : 2, spectrum *1*) suggests that the PO_4 tetrahedron is strongly distorted like HPO_4. Many bands in the range 1250–890 cm^{-1} and comparable intensities of bands at 1117–1082 and 1030–1040 cm^{-1} for P–Sb samples point to the presence of PO_4 tetrahedrons of two types (with longer and shorter P–O bonds). The low-frequency component (950–1070 cm^{-1}) can be assigned to antimony phosphate with a high probability.

The band at 880–810 cm^{-1} is most likely due to the stretching vibrations of the P–O–Sb groups. The bands at 660–460 cm^{-1} belong to the deformational vibrations of PO_4 groups and to the stretching and deformational vibrations of Sb–O bonds. Note that, the sample with Sb : P = 15 : 1, which contains a significant excess of antimony, has absorption bands at 290, 367, 447, 498, 528, 610, 670, 745, and 762 cm^{-1}, which correspond to the spectrum of Sb_2O_4 [33].

Comparison of the spectra for the catalyst, pure gallium antimonate, and model P–Sb samples shows that the multicomponent catalyst contains a compound with a structure of gallium antimonate in which the lengths of *M*–O bonds are changed compared to pure gallium antimonate. The presence of PO_4 and P–O–Sb groups suggests the stabilization of phosphate ions in the catalyst structure.

The electron microscopic images (Fig. 5a) made with low magnification to determine the shape and size of catalyst particles show that the catalyst particles have a round form and a size of 20–25 nm. At a higher magnification (Fig. 5b), we observed the catalyst microstructure in more detail. The catalyst is nanostructured. The particles of SiO_2 (20–25 nm) are almost completely and uniformly coated with noncoherently spliced crystalline particles with lattice parameters that

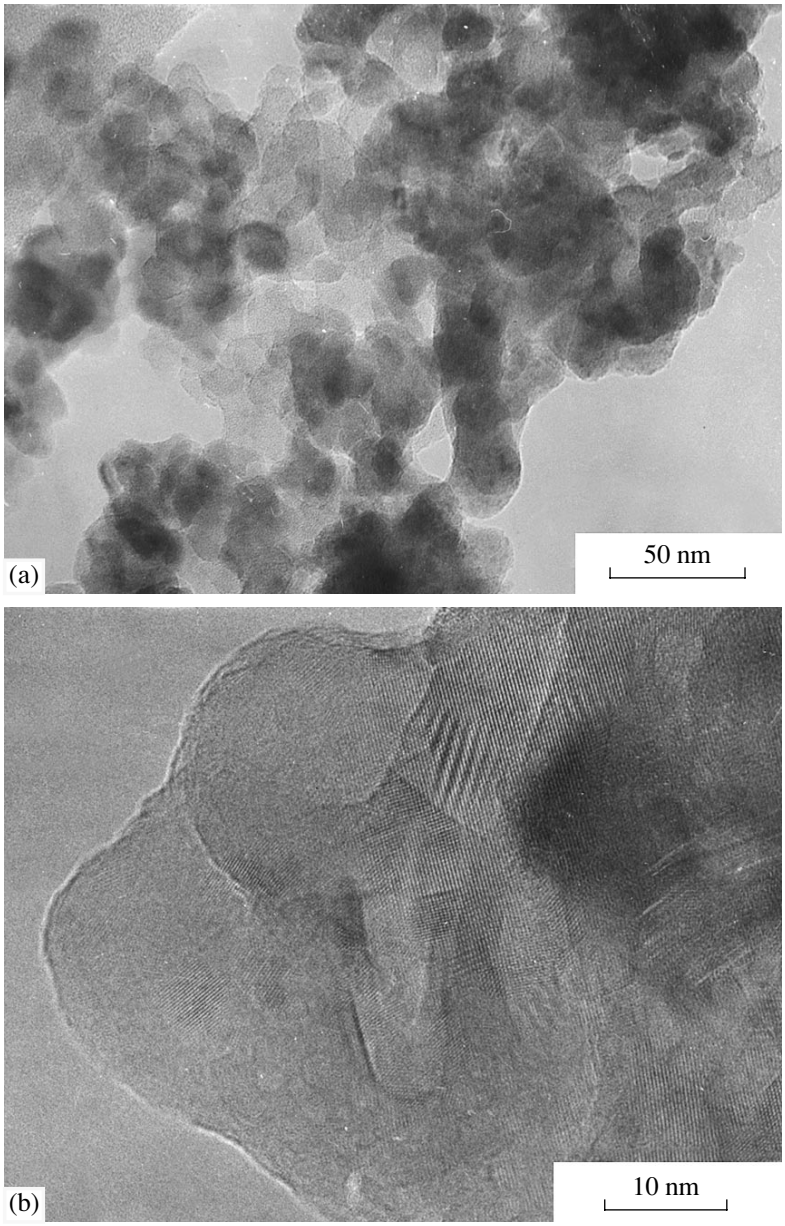

Fig. 5. Electron microscopic patterns of the $Ga_1Ni_1P_2W_{0.5}Sb_6O_x/SiO_2$ catalyst with different magnifications.

are close to the structure of gallium antimonate. The coating layer thickness is about 10 nm. We clearly saw the boundaries of blocks between noncoherently spliced particles with a structure of gallium antimonate. The size of a separate block is 5–7 nm according to electron microscopy, which is close to the size of CSR determined by XRD. We did not find any other crystalline or X-ray amorphous phases in the catalyst by electron microscopy.

Table 2. Catalytic properties of the $Ga_1Ni_1P_2W_{0.5}Sb_6O_x/SiO_2$ and $Ga_1Ni_3P_2W_{0.5}Sb_6O_x$ systems in propane ammoxidation

Catalyst	Conversion, %	Selectivity, %					C_3H_3N yield, %
		CO_2	CO	C_2H_3N	C_3H_3N	HCN	
$Ga_1Ni_1P_2W_{0.5}Sb_6O_x/SiO_2$	90.4	15.6	14.6	1.5	60.7	7.7	54.9
$Ga_1Ni_3P_2W_{0.5}Sb_6O_x$	83.4	18.0	14.6	1.6	60.1	5.7	50.2

Comparison of these data with IR spectroscopic and XRD data allows us to assume that phosphate ions are stabilized in the region of block boundaries with the formation of the fragments of P–Sb molecular-size compounds. This is possible because the noncoherent splicing of blocks in the region of block boundaries makes the crystalline lattice of a gallium antimonate-based compound irregular and stabilizes phosphate ions in the tetrahedral coordination.

Note that attempts to obtain a single-phase system in massive catalysts that were prepared by the precipitation method with a similar elemental composition but a slightly different component ratio ($Ga_1Ni_3P_2W_{0.5}Sb_6O_x$) have been unsuccessful. According to [24], a mixture of phases was observed for this catalyst. These phases were assigned to gallium and nickel antimonates and an X-ray amorphous P–Sb compound. This is probably due to the fact that an increase in the concentration of nickel in such a multicomponent catalyst leads to a change in the stability of the phase with the gallium antimonate structure. Our catalyst preparation method probably provides better binding of all catalyst components.

Table 2 shows the catalytic properties of $Ga_1Ni_1P_2W_{0.5}Sb_6O_x/SiO_2$ in the reaction of propane ammoxidation. Similar data for the $Ga_1Ni_3P_2W_{0.5}Sb_6O_x$ catalyst [24, 25] are given for comparison. It is seen that the former catalyst shows somewhat higher activity and selectivity to acrylonitrile, and the yield of acrylonitrile is higher. These differences can be due to different phase compositions and structural properties of these two catalysts. The nanostructured catalyst with a single phase of gallium antimonate structure is more efficient than the catalyst consisting of mixed phases (gallium and nickel antimonates and a P–Sb compound).

CONCLUSION

Thus, the $Ga_1Ni_1P_2W_{0.5}Sb_6O_x/SiO_2$ catalyst obtained by mixing a P–Sb compound, the solutions of other components, and SiO_2 becomes nanostructured after drying and thermal treatment at 750°C, because it consists of noncoherently spliced crystallites of a compound with a gallium antimonate structure. In the structure of the multiply promoted compound based on gallium antimonate, the Ni^{2+} ions partially substitute for the Ga^{3+} ions, and the W^{6+} ions substitute for the Sb^{5+} ions. The phosphate ions are stabilized in the region of block boundaries. The blocks of the compound uniformly cover the SiO_2 particles. The resulting catalyst is rather efficient in propane ammoxidation.

ACKNOWLEDGMENTS

We thank S.Yu. Burylina and Z.G. Osipova for testing the catalytic properties of the samples.

REFERENCES

1. Centi, G., Grasselli, R.K., and Trifiro, F., *Catal. Today*, 1992, vol. 13, no. 4, p. 661.
2. Cassidy, T.J., Pollastri, M., and Trifiro, F., *J. Catal.*, 1997, vol. 172, no. 1, p. 55.
3. Nilsson, R., Lindblad, T., Andersson, A., Song, S., and Hansen, S., *Stud. Surf. Sci. Catal.*, 1994, vol. 82, p. 293.
4. Centi, G., Grasselli, R.K., Patane, E., and Trifiro, F., *Stud. Surf. Sci. Catal.*, 1990, vol. 55, p. 515.
5. Nilsson, J., Landa-Canovas, A.R., Hansen, S., and Anderson, A., *Stud. Surf. Sci. Catal.* 1997, vol. 110, p. 413.
6. Nilsson, R., Lindblad, T., and Andersson, A., *J. Catal.*, 1994, vol. 148, no. 2, p. 501.
7. Nilsson, R., Landa-Canovas, A.R., Hansen, S., and Anderson, A., *J. Catal.*, 1996, vol. 160, no. 2, p. 244.
8. Hansen, S., Stähl, K., Nilsson, R., and Andersson, A., *J. Solid. State. Chem.*, 1993, vol. 102, no. 2, p. 340.
9. Landa-Canovas, A., Nilsson, J., Hensen, S., Stähl, H., and Andersson, A., *J. Solid State Chem.*, 1995, vol. 116, no. 2, p. 369.
10. Centi, G. and Mazzoli, P., *Catal. Today*, 1996, vol. 28, no. 4, p. 351.
11. Ratajczak, O., Zanthoff, H.W., and Geisler, S., *Stud. Surf. Sci. Catal.*, 2000, vol. 130, p. 1685.
12. Boudeville, Y., Figueras, F., Forissier, M., Portefaix, J.I., and Vedrine, J.C., *J. Catal.*, 1979, vol. 58, no. 2, p. 52.
13. Nilsson, J., Landa-Canovas, A.R., Hansen, S., and Anderson, A., *Catal. Today*, 1997, vol. 33, nos. 1–3, p. 97.
14. Albonetti, S., Blanchard, G., Burattin, P., Cavani, F., Masetti, S., and Trifiro, F., *Catal. Today*, 1998, vol. 42, no. 3, p. 283.
15. Albonetti, S., Blanchard, G., Burattin, P., Cavani, F., Masetti, S., and Trifiro, F., *Stud. Surf. Sci. Catal.*, 1997, vol. 110, p. 403.
16. Herniman, H.J., Pyke, D.R., and Reid, R., *J. Catal.*, 1979, vol. 58, no. 1, p. 68.
17. Cross, Y.M. and Pyke, D.R., *J. Catal.*, 1979, vol. 58, no. 1, p. 61.
18. Osipova, Z.G. and Sokolovskii, V.D., *React Kinet. Catal. Lett.*, 1978, vol. 9, no. 2, p. 193.
19. Osipova, Z.G. and Sokolovskii, V.D., *Kinet. Katal.*, 1979, vol. 20, no. 4, p. 910.
20. Burylin, S.Yu., Osipova, Z.G., and Sokolovskii, V.D., *Kinet. Katal.*, 1983, vol. 24, no. 3, p. 639.
21. Burylin, S.Yu., Osipova, Z.G., Sokolovskii, V.D., Kalinkin, A.V., Pashis, A.V., Shubin, A.A., and Olen'kova, I.P., *Kinet. Katal.*, 1990, vol. 31, no. 5, p. 1271.
22. Burylin, S.Yu., Osipova, Z.G., Sokolovskii, V.D., Olen'kova, I.P., Kalinkin, A.V., and Pashis, A.V., *Kinet. Katal.*, 1989, vol. 30, no. 4, p. 494.
23. Burylin, S.Yu., Osipova, Z.G., Sokolovskii, V.D., and Olen'kova, I.P., *Kinet. Katal.*, 1989, vol. 30, no. 5, p. 1251.
24. Burylin, S.Yu., Osipova, Z.G., Sokolovskii, V.D., and Olenkova, I.P., *React. Kinet. Catal. Lett.*, 1981, vol. 18, nos. 1–2, p. 7.

25. Sokolovskii, V.D., Davidov, A.A., and Ovsitser, O.Yu., *Catal Rev.–Sci. Eng.*, 1995, vol. 37, no. 3, p. 425.

26. Zenkovets, G.A., Tarasova, D.V., and Olen'kova, I.P., *Izv. Sib. Otd. Akad. Nauk SSSR, Ser. Khim. Nauk.*, 1984, no. 4, p. 45.

27. Tsybulya, S.V., Cherepanova, S.V., and Solov'eva, L.P., *Zh. Strukt. Khim.*, 1996, vol. 37, no. 2, p. 379.

28. Iveronova, V.I. and Revkevich, G.P., *Teoriya rasseyaniya rentgenovskikh luchei* (Theory of X-ray Scattering), Moscow: Mosk. Gos. Univ., 1978.

29. JCPDS Data File 33-0100.

30. Lever, A.B.V., *Inorganic Electronic Spectroscopy*, Amsterdam: Elsevier, 1984, vol. 2.

31. Mott, N.F. and Davis, E.F., *Electronic Processes in Non-crystalline Materials*, Oxford: Oxford Univ. Press, 1979, vol. 1.

32. Karapet'yants, M.Kh. and Drakin, S.I., *Stroenie veshchestva* (Structure of Matter), Moscow: Vysshaya Shkola, 1967, p. 81.

33. Pechkovskii, V.V., Mel'nikova, R.Ya., Dzyuba, E.D., Barannikova, T.I., and Nikanovich, M.V., *Atlas infrakrasnykh spektrov fosfatov. Ortofosfaty* (Atlas of Infrared Spectra of Phosphates: Orthoposphates), Moscow: Nauka, 1981.